Effect of hydrophilicity-imparting substituents on exciton delocalization in squaraine dye aggregates covalently templated to DNA Holliday junctions†

Gissela Pascual, [ID] [a] Simon K. Roy, [ID] [a] German Barcenas, [a] Christopher K. Wilson, [a] Keitel Cervantes-Salguero, [ID] [a] Olena M. Obukhova, [b] Alexander I. Krivoshey, [b] Ewald A. Terpetschnig, [c] Anatoliy L. Tatarets, [b] Lan Li, [a] Bernard Yurke, [a,d] William B. Knowlton, [a,d] Olga A. Mass, [ID] [a] Ryan D. Pensack [ID] [a] and Jeunghoon Lee [ID] *[a,e]

Molecular aggregates exhibit emergent properties, including the collective sharing of electronic excitation energy known as exciton delocalization, that can be leveraged in applications such as quantum computing, optical information processing, and light harvesting. In a previous study, we found unexpectedly large excitonic interactions (quantified by the excitonic hopping parameter $J_{m,n}$) in DNA-templated aggregates of squaraine (SQ) dyes with hydrophilic-imparting sulfo and butylsulfo substituents. Here, we characterize DNA Holliday junction (DNA-HJ) templated aggregates of an expanded set of SQs and evaluate their optical properties in the context of structural heterogeneity. Specifically, we characterized the orientation of and $J_{m,n}$ between dyes in dimer aggregates of non-chlorinated and chlorinated SQs. Three new chlorinated SQs that feature a varying number of butylsulfo substituents were synthesized and attached to a DNA-HJ *via* a covalent linker to form adjacent and transverse dimers. Various characteristics of the dye, including its hydrophilicity (in terms of log $P_{o/w}$) and surface area, and of the substituents, including their local bulkiness and electron withdrawing capacity, were quantified computationally. The orientation of and $J_{m,n}$ between the dyes were estimated using a model based on Kühn–Renger–May theory to fit the absorption and circular dichroism spectra. The results suggested that adjacent dimer aggregates of all the non-chlorinated and of the most hydrophilic chlorinated SQ dyes exhibit heterogeneity; that is, they form a mixture of dimers subpopulations. A key finding of this work is that dyes with a higher hydrophilicity (lower log $P_{o/w}$) formed dimers with smaller $J_{m,n}$ and large center-to-center dye distance ($R_{m,n}$). Also, the results revealed that the position of the dye in the DNA-HJ template, that is, adjacent or transverse, impacted $J_{m,n}$. Lastly, we found that $J_{m,n}$ between symmetrically substituted dyes was reduced by increasing the local bulkiness of the substituent. This work provides insights into how to maintain strong excitonic coupling and identifies challenges associated with heterogeneity, which will help to improve control of these dye aggregates and move forward their potential application as quantum information systems.

[a]Micron School of Materials Science & Engineering, Boise State University, Boise, Idaho 83725, USA
[b]State Scientific Institution "Institute for Single Crystals" of the National Academy of Sciences of Ukraine, Kharkiv 61072, Ukraine
[c]SETA BioMedicals, LLC, Urbana, Illinois 61801, USA
[d]Department of Electrical & Computer Engineering, Boise State University, Boise, Idaho 83725, USA
[e]Department of Chemistry and Biochemistry, Boise State University, Boise, Idaho 83725, USA. E-mail: jeunghoonlee@boisestate.edu
†Electronic supplementary information (ESI) available. See DOI: https://doi.org/10.1039/d3nr04499h

1. Introduction

Molecules (*i.e.*, dyes) can form aggregates through non-covalent interactions, such as electrostatic forces and van der Waals interactions, and exhibit unique optical characteristics due to collective sharing of electronic excitation energy. The collective resonance interaction among excited states of coupled molecules within dye aggregates results in exciton delocalization or Frenkel excitons.[1–4] Excitons in the photosynthetic machinery, created by the photo-excitation of the molecular aggregates, have inspired extensive research interest in energy conversion, opening new horizons to next-generation technology. Some examples include artificial light-harvesting,[2,5] nanoscale computing using quantum gates,[4,6–8]

and biological and environmental sensing.[9,10] In a recent review, Mathur *et al.*[11] suggested that quantum computing may be the most extensive impactful application of exciton delocalization, using methodologies provided by Yurke.[4,8]

Based on Frenkel exciton theory, Kasha proposed the excitonic model that describes how exciton interaction depends on the orientation of the transition dipole moment (TDM) vectors of at least two molecules (*m* and *n*).[1] These dye molecules contain chromophores that provides them with optical activity. The excitonic hopping parameter ($J_{m,n}$), also known as the excitonic exchange energy or intermolecular coulombic interaction parameter,[12] measures the strength of excitonic interaction. $J_{m,n}$ depends on the orientation of the TDM associated with each molecule within the aggregate. The excitonic coupling model is used to predict the geometry of molecular aggregates based on the resulting exciton states and optical transitions between these states (Fig. 1).[1,13] This model proposes three types of aggregates: J-aggregates, H-aggregates, and oblique aggregates. J-aggregates consist of molecules with TDMs aligned in an end-to-end manner. They display red-shifted (bathochromic) absorption spectra because the only optically allowed electronic transition is from the ground state to the lowest-energy exciton state. Sometimes J-aggregates feature narrow absorption spectral widths, small Stokes shift, and, in principle, shortened excited state lifetimes due to superradiance.[14] H-aggregates consist of molecules with TDMs aligned in a face-to-face manner. They generally exhibit blue-shifted (hypsochromic) absorption spectra because the optically allowed electronic transition is from the ground state to the highest-energy exciton state. H-aggregates have also been found to exhibit narrow absorption spectral widths[15] and, in

contrast to J-aggregates, the H-aggregates are expected to have longer excited state lifetimes due to subradiance (although in practice this is rarely found to be the case).[14] Some dyes (*e.g.*, quadrupolar conjugated) might form H-aggregates that exhibit red-shifted absorption spectra.[16,17] Oblique aggregates are an intermediate configuration that are formed by the perpendicular arrangement of TDMs;[1] in this case, optical transitions from the ground state to both lower and higher energy exciton states are allowed.

The spontaneous aggregation of dyes *via* non-covalent interaction is sensitive to the characteristics of the solvent,[18] ionic strength,[19] temperature,[20] and polarity.[21] Although many dyes self-assemble in solution under appropriate conditions,[18–21] the absence of a template makes it difficult to control the geometric arrangement and number of participant dyes in the aggregation. In photosynthetic complexes of plants and bacteria, protein templates enable efficient electronic excitation energy transfer by controlling the geometry of the molecular aggregates and their exciton delocalization. Proteins facilitate the highly compact packing of molecules, known as pigments, enabling strong coupling and energy tuning *via* molecule-protein interaction.[22] Nonetheless, the design of synthetic protein scaffold-based nanoarchitectures for controlling the molecular interaction is still challenging due to many amino acid combinations and complex folding mechanisms. In contrast, sequences of deoxyribonucleic acid (DNA) strands are composed of only four types of bases (adenine, cytosine, guanine, and thymine) which hybridize to form a stable DNA duplex bound by Watson–Crick base pairing between complementary nucleobases.[23–25] The development of solid-supported synthesis of DNA strands facilitates easy programmabi-

Fig. 1 The Frenkel molecular exciton model described by Kasha[1] shows the energy transition of dimer aggregates (J-aggregate, oblique, and H-aggregate) relative to the monomer. A monomer shows the transition from the ground energy state ($E°$) to the first excited energy state. The formation of aggregates induces exciton delocalization, splitting the excited energy state into higher (E'') and lower (E'). Dashed arrows indicate the forbidden energy transition. Arrows inside molecules represent the transition dipole moment (TDM); the TDMs of an oblique dimer is perpendicular.

lity of the base sequences, enabling control over the intermolecular affinity.[23,26] Current advances in nanotechnology allow the synthesis of branched DNA nanostructures such as four-arm DNA Holliday junctions (DNA-HJ) that are composed of crossover strands with specifically designed base sequences and a fixed branching center.[23] Unique sequences with non-complementary bases in the vicinity of the branch point prevent branch migration, making the DNA-HJ immobile and more stable.[25] Dyes can be non-covalently and covalently assembled along the DNA strands. Non-covalent binding allows molecular assembly by intercalating dyes between the nucleobase pairs[27] or by binding into the grooves,[28,29] but the control over position and orientation of the participant dyes in the aggregate is difficult. In contrast, the covalent binding is more advantageous over non-covalent binding due to the robust dye assembly[26,30] with accurate positioning[26] along the DNA strands. Hence, the covalent attachment of dyes to DNA enables the control of the geometry of and $J_{m,n}$ between dyes in dye aggregates, yet these properties can still be influenced by the neighboring nucleobases.[31]

During the last decade, squaraine (SQ) and cyanine (Cy) dyes attached to DNA structures have been extensively investigated for their ability to form aggregates and exhibit exciton delocalization.[12,29,32–44] SQs and Cys exhibit unique optical properties, such as intense light absorption and fluorescence emission in the visible (VIS) and near-infrared (NIR) spectral regions.[45–47] Unlike Cys, SQs have an electron-deficient squarate moiety at the center of the pentamethine chain that bridges the electron-rich indolenine rings, which confers a donor–acceptor-donor (D–A–D) structure.[41,48] The squarate moiety also makes the bridge rigid and planar, suppressing photoisomerization and oxidation compared to dyes with only a polymethine chain; in these respects, this structural modification improves the photostability of SQs compared with Cys. Moreover, SQs are tunable by functionalizing the D and A moieties[46] with diverse types of substituents for distinct optical and electronic properties. In fact, additional dye properties are impacted by the characteristics of the substituents on the dye periphery.[28,34,43] Studies demonstrated that dye–dye aggregation relies on the inherent properties of the dyes such as hydrophobicity,[28,34] steric hindrance (bulkiness of the substituents),[43] and the dye position within the template.[32,34,43]

The aggregation of dyes templated by DNA leading to exciton delocalization has been extensively studied.[12,28–30,32–44,49] A few experimental studies using Cys[28,43] and SQs[34] addressed the influence of dye substituents on the optical properties of DNA-templated molecular aggregates. An earlier study of the hydrophobicity effect on the aggregate formation was conducted by Stadler et al.[28] using Cy functionalized with methoxy groups or fluorine atoms in which the Cys accumulated into the minor grooves of DNA duplexes. The authors found that dyes symmetrically substituted with methoxy groups promoted stronger aggregate formation than those functionalized with fluorine atoms, but the precise geometry of the aggregates was not reported. Recently, our group investigated the orientation of and $J_{m,n}$ between dyes

in dimers and tetramers of a series of six different SQs divided in two sets of hydrophobic and hydrophilic dyes based on their octanol/water partition coefficient ($\log P_{o/w}$).[34] The SQ dyes were attached to two complementary or non-complementary strands of the DNA-HJ, via a single flexible 6-carbon linker, to form adjacent or transverse dimers, respectively. The result from hydrophobic dye aggregates confirmed that hydrophobicity promotes their aggregation and exciton delocalization by reducing the center-to-center distance between the dyes and increasing $J_{m,n}$. Larger $J_{m,n}$ was observed for the adjacent dimers as compared with the transverse dimers. Aggregates of the most hydrophobic SQ dye with two chlorine atoms ($SQ\text{-}Cl_2$) exhibited the largest $J_{m,n}$ (132 meV)[34] as estimated by our in-house KRM Model Simulation tool based on Kühn–Renger–May theory.[50] However, hydrophilic dyes with hydrophilic-imparting substituents sulfo (-Sl) and butylsulfo (-buSl) substituents attached to indolenine rings also exhibited aggregation and $J_{m,n}$ comparable to hydrophobic dye aggregates. Surprisingly, $SQ\text{-}Sl_5$ that has two -Sl and three -buSl substituents, which was classified overall as the most hydrophilic via its $\log P_{o/w}$, exhibited a considerably large $J_{m,n}$ (97 meV).[34] We suspected that the butyl chains in -buSl substituent increased hydrophobic interactions and promoted the unexpected aggregation of these hydrophilic dyes. Meanwhile, Díaz et al.[43] demonstrated that steric hindrance, and to a lesser extent the hydrophobicity, exerts a strong influence on $J_{m,n}$ between symmetrically substituted Cy5s attached to DNA-HJ via 3-carbon linker two-point attachment linkers. In contrast to SQs,[34] larger $J_{m,n}$ between Cy5s[32,43] was reported for transverse dimers potentially due to the different way in which the dyes were attached to the DNA strands.

Previous studies provided valuable starting points for understanding the dependence of aggregation and $J_{m,n}$ on dye structure. However, further studies are required to better understand the influence of hydrophilicity and steric effects on $J_{m,n}$ and geometry of dye aggregates. The unexpected aggregation of SQs and their large $J_{m,n}$ by increasing the number of hydrophilic-imparting substituents found in our previous work[34] prompted us to investigate an expanded set of SQ dyes. The spatial distribution of substituents around the SQs, either symmetrically or asymmetrically, could play a role in their aggregation propensity or influence their packing geometry. In addition, the position of the SQ-DNA linker could influence the packing and $J_{m,n}$ due to the hydrophobic interaction between the aliphatic linker and the aliphatic chain in a -buSl substituent. The present study introduced three new SQs featuring chlorine atoms (-Cl) and -buSl substituents to further our understanding gained from our previous work on the aggregation propensity of SQs, hence $J_{m,n}$.[34] This work followed the general hypothesis that hydrophilicity reduces the tendency for molecular aggregation, and hence $J_{m,n}$, because of the reduced SQ-SQ interactions due to higher affinity of such dyes to water. $\log P_{o/w}$ was calculated, along with solvent-accessible surface area (SASA) to gain insights into the characteristics of SQs. The characteristics of substituents, such as their local bulkiness and electron withdrawing capacity, might also

play a role in aggregation and $J_{m,n}$. Thus, local bulkiness (*A*-value) was calculated and their electron withdrawing capacity from literature was used to gain insight into the characteristics of hydrophilic imparting substituent.onSQs templated by DNA-HJ, attaching the SQs to the DNA *via* a single flexible linker. $J_{m,n}$ between and orientation of the dyes in the dimers were estimated using our KRM model simulation tool; an approach is proposed here to evaluate the presence of single or multiple types of aggregates. In addition, the position of the SQ-DNA linker was changed to investigate the influence of linker position on the $J_{m,n}$ and dye packing.

2. Material and methods

2.1. Squaraine dye synthesis and preparation of SQ-DNA constructs

The synthesis of the SQs, *SQ-H₂, SQ-Sl₂, SQ-Sl₃,* and *SQ-Cl₂* that are hereafter labeled as *a-1*, *a-2*, *a-3*, and *b-1*, respectively, was reported previously.[34] SQ-Sl₅ of our previous study was not included in the present work due to the presence of a significant amount of optical monomer in the transverse dimer solution at room temperature. These SQs feature hydrophilic-imparting substituents -*Sl* and -*buSl*. In the present work, the set of dyes was expanded to include three newly synthesized SQs (*b-2*, *b-3*, and *b-4*), which feature -*Cl* and -*buSl* substituents (these dyes are hereafter called chlorinated SQs). The synthesis of the new chlorinated SQs that include -*buSl* substituents is reported in the ESI (section SI 1†). The previous finding of our group that aggregates of *b-1* have the strongest excitonic interactions (highest $J_{m,n}$)[34] among hydrophobic SQs[34] prompted the synthesis and further investigation of sulfonated SQ variants such as *b-2*, *b-3*, and *b-4*. Thus, two groups of SQs featuring -*Sl* and -*buSl* with their respective controls, were analyzed in the present work (Fig. 2A). The first group is non-chlorinated SQs (*a-1*: control, *a-2*, and *a-3*), and the second group is chlorinated SQs (*b-1*: control, *b-2*, *b-3*, and *b-4*).

The newly synthesized SQs were covalently attached to the DNA strands, *via* a single flexible linker, by Integrated DNA Technologies, Inc. and dehydrated until use in downstream experiments. Stock solutions of SQ-DNA at 100 μM were hydrated using ultrapure water (Barnstead Nanopure, Thermo Scientific). The concentration of SQ-DNA was calculated based on the absorbance at 260 nm measured using NanoDrop (Thermo Scientific) and the extinction coefficient of the associated DNA absorption band provided by the supplier.

Monomers of *b-2*, *b-3*, and *b-4* and six unique SQ dimers templated by immobile DNA-HJ (Fig. 2B and Table S1†) were prepared using equimolar concentrations (1.5 μM) of four complementary DNA strands (labeled with and without SQs) in 1× TBE, 15 mM MgCl₂ buffer solution. The monomers have one SQ in the strand A, the adjacent dimers have one SQ in two complementary DNA strands (strands B and C), and the transverse dimers have one SQ in two non-complementary DNA strands (strands A and C). Each DNA strand has 26 bases, except the strands labeled with one SQ because they have an

additional thymine (14th base position) used to link the SQ *via* a covalent bond (Fig. 2A and section SI 2†). DNA constructs were annealed in an attempt to achieve the homogeneous formation of the target structure. During the annealing process, the samples were heated at 95 °C (4 min), gradually cooled down until 64 °C, and then gradually cooled down to room temperature. Samples were stored at 4 °C until use in experiments.

2.2. Optical characterization of SQ-DNA constructs

Steady-state absorption of SQ-DNA constructs (monomers and dimer) was recorded at room temperature (22 °C) using a UV-Vis-NIR absorption spectrophotometer (Agilent, Cary 5000) in dual-beam mode. The SQ-DNA construct solution (1.5 μM) was contained in a 50 μL capacity quartz cuvette of 1 cm path length. Absorption spectra were recorded twice from 230 to 800 nm wavelength in 1 nm steps.

Circular dichroism (CD) of the SQ-DNA constructs was measured using a spectropolarimeter (J-1500, JASCO). The solution of SQ-DNA construct (1.5 μM) was contained in a 100 μL capacity quartz cuvette (Starna cells) of 1 cm path length. CD spectra were recorded from 230 to 800 nm three times at 200 nm min⁻¹.

Steady-state fluorescence spectra were recorded using a fluorescence spectrometer (Fluorolog-3, Horiba Scientific) with the sampled contained in a 1 cm path-length quartz cuvette (Starna cells). Details of additional experimental parameters, such as excitation wavelength, are reported where appropriate.

2.3. Characterization of squaraine dyes and their substituents

SQs were characterized by theoretically calculating the octanol/water partition coefficient ($\log P_{o/w}$) which we use as a general proxy for the overall hydrophilicity of the SQ, and the solvent accessible surface area (SASA). In this work, $\log P_{o/w}$ was calculated following the approach described by Garrido *et al.*,[51] which is the same approach used for non-chlorinated dyes and the *b-1* SQ.[34] Log $P_{o/w}$ was calculated based on the absolute solvation Gibbs energies[51] using the Gaussian software package[52] following eqn (1). It is the negative value of the difference of solvation energies between *n*-octanol (ΔG_o) and water (ΔG_w) calculated using density functional theory (DFT)[53] divided by 2.3 times the gas constant ($R = 8.31$ J mol⁻¹ K⁻¹) and temperature ($T = 273.15$ K). More negative and more positive $\log P_{o/w}$ values indicate more hydrophilic and hydrophobic behavior of SQs, respectively.

$$\log P_{o/w} = -\frac{\Delta G_o - \Delta G_w}{2.303RT} \tag{1}$$

The molecular geometry of SQ was initially approximated using the force fields model (UFF)[54] using Avogadro[55] open license software. Then, structures were optimized using Gaussian 16 software package with the 6-31+G (d,p) basis set with the M06-2X exchange correlation functional.[56]

The optimized SQ structures in water were used to calculate the SASA for the entire dye. SASA was calculated by using the

Fig. 2 Chemical structure of the non-chlorinated and chlorinated squaraine dyes (SQs) and the modifications of their functional groups. (A) SQ (with linker and thymine sequence modifier plus linker) shows the places of the substituents. (B) Schematic representation of SQs monomers and dimers in DNA-HJ. (C) Schematic representation of molecular interaction to understand the geometry of dimers templated by the DNA-HJ (see variables in Table 4).

optimized ground state structure inside of the ChimeraX[57] software package and using the measured SASA function. Increased SASA (Å^2) indicates a larger dye surface area that is accessible by the solvent (water), but this increased SASA does not necessarily indicate a higher affinity to water. The affinity to water of a dye is assessed using $\log P_{\text{o/w}}$. The SASA and hydrophilicity are characteristics of SQs described by the number of substituents and their identity such as chlorine

atoms (-Cl) and sulfonic acid (sulfo) -SO_3H (-Sl) and butylsulfo -$(CH_2)_4SO_3H$ (-$buSl$) groups.

The local bulkiness or steric hindrance of substituents of SQ was quantified by the A-value, which measures the difference in energy between the equatorial and axial conformation of cyclohexane in the presence of the substituent. A high A-value of SQs generated using the Gaussian software package[52] characterizes locally bulkier substituents. The free

energy of each SQ was taken from the thermochemical data produced during the frequency calculation of each SQ without solvent. The output was analyzed with the cclib Python library.[58]

2.4. KRM modeling and data analysis

The orientation of and $J_{m,n}$ between dyes in SQ aggregates were calculated using the in-house-developed KRM model simulation tool (version ev13v5, 2022). The KRM modeling tool simultaneously fits absorbance and CD spectra to estimate orientation of and $J_{m,n}$ between dyes in the aggregate (Fig. 2C). Absorption and CD spectra data of SQ-DNA constructs in solution were collected at room temperature to prevent an influence of temperature[20] on the dye aggregation. In previous studies, the KRM model simulation tool has been successfully applied to calculate the geometry of and $J_{m,n}$ between dyes in dye aggregates.[12,32–34,43] The theoretical formulation[50] for the KRM model was described in detail by Roy *et al.*[33] Briefly, the KRM model uses the TDM vector length (1.3 nm) and absorption spectrum (in extinction coefficient), to find the fitting parameters of a monomer such as the energy a vibron (eV), the displacement of the excited state potential from the ground state potential (d), and the energy loss parameter (Γ). These parameters allow the tool to calculate the TDM amplitude of the monomer in units of Debye (D) along with the characteristic exciton hopping parameter (J_0) in units in millielectronvolts (meV). J_0 is a constant pre-factor for calculation of $J_{m,n}$.[33] CD of monomers is not needed because only aggregates are expected to exhibit CD signal. However, the CD of monomers is not necessarily zero as shown for SQs[34] but essentially is negligible.[59] Using the features of the monomers and offset energy of dimers (Eof), allows the calculation of $J_{m,n}$ between dyes and the dye aggregate packing geometry by simultaneously modeling their absorption and CD spectra. The KRM modeling tool calculates the shortest distance ($d_{m,n}$) between the two TDM vectors of the dyes (approach of single dimer) using a limited distance of 0.34 nm. This minimum distance was chosen based on the minimum distance between SQs (0.35 nm) in single crystals of indolenine-based selenium-substituted SQs.[60]

In this study, single (homogeneous) *versus* multiple (heterogeneous) populations of aggregate structures in solution were examined using a new KRM modeling approach. First, the optical properties are modeled using a single population of aggregates, which uses two TDM vectors, one for each dye in the dimer. If the result shows that the normalized overlap integral of the experimental and theoretical absorption and CD spectra are high (*e.g.*, ≥ 90%), the dimer is assigned as a single type of dimer population. However, if the normalized overlap integral of the experimental and theoretical absorption and CD spectra are low (*e.g.*, ≤ 90%), an intensive KRM modeling was performed following a new approach that accounts for a heterogeneous population of aggregate types. The new approach uses four TDM vectors for two dimer populations. The distance between dimers was set to 1 μm to ensure that $J_{m,n}$ between dyes in the separated dimers is effectively zero.

This distance is reasonably expected for dye aggregates sufficiently separated from each other due to the size of the DNA-HJ and the electrostatic repulsion imposed by the DNA duplexes. The best fit between the two modeling approaches was determined based on the higher value of normalized overlap integral of both experimental and theoretical data. A significant fitting improvement was observed for adjacent dimers *a-1*, *a-2*, and *a-3* when using the heterogeneous population approach as compared with the previously used single type of dimers approach.[34]

The relationship between the maximum $J_{m,n}$ and dye properties (*e.g.*, water affinity) was evaluated using linear regression analysis, in which the coefficient of determination *R*-square (R^2) is scaled from 0 to 1. This coefficient represents the proportion of variation in $J_{m,n}$ that can be explained by the properties of SQs.

3. Results and discussion

3.1. Structural characteristics and physical properties of squaraine dyes (SQs)

The present work used chlorinated and non-chlorinated sets of SQs with their respective controls *a-1* and *b-1* (Fig. 2A). The physical properties of SQs, such as ΔG_w and ΔG_o, log $P_{o/w}$, and SASA, rely on the structural characteristics of the substituents (Table 1). The structural characteristics and physical properties of the non-chlorinated SQs (*a-1, a-2,* and *a-3*) and the chlorinated SQ *b-1* were described in our previous study.[34] Here, we first briefly compared the properties between *a-1* and *b-1*. Then, we compared the SQs, that featured hydrophilic-imparting substituents, with their respective controls to give context of KRM modeling in section 3.4.

The control dyes *a-1* and *b-1* have H and Cl atoms, respectively, at positions 5- and 5′- in the indolenine rings. Compared to *a-1* (ΔG_w = −79, ΔG_o = −102 kJ mol⁻¹), *b-1* exhibits a reduced solvation energy in water and octanol (ΔG_w = −82, ΔG_o = −110 kJ mol⁻¹). Changes in the ΔG resulted in a higher log $P_{o/w}$ for *b-1* (5.31) as compared with *a-1* (4.30), revealing that *b-1* had less affinity to water (less hydrophilic) than *a-1*. The less hydrophilic behavior of *b-1* arises from the chlorine atoms that also increase the SASA from 665 Å² (*a-1*) to 740 Å² (*b-1*), reflecting the larger atomic size of chlorine compared with hydrogen.

Non-chlorinated SQs *a-2* and *a-3* have -*Sl* at positions 5- and 5′- in the indolenine rings as compared with *a-1* (Fig. 2A). Additionally, *a-3* has a -*buSl* group at position 1 in the indolenine ring. Compared with *a-1*, lower log $P_{o/w}$ values were obtained for *a-2* and *a-3.* The presence of two -*Sl* groups in *a-2* as compared with two hydrogen atoms in *a-1* caused ΔG_w to decrease from −79 to −181 kJ mol⁻¹ and ΔG_o to decrease from −102 to −161 kJ mol⁻¹. Likewise, the log $P_{o/w}$ was reduced from 4.30 to −3.66. The larger SASA of *a-2* (825 Å²) than *a-1* (665 Å²) reflects the larger structural size of -*Sl* than -*H*. The additional presence of the -*buSl* group in *a-3* further reduced both ΔG_w and ΔG_o (Table 1). Thus, *a-3* resulted in the most

Table 1 Characteristic of squaraine dyes (SQs) using theoretical approaches

Dye group		Dye	$\Delta G_{\mathrm{w}}{}^{a}$ [kJ mol^{-1}]	$\Delta G_{\mathrm{o}}{}^{b}$ [kJ mol^{-1}]	Log $P_{\mathrm{o/w}}{}^{c}$	SASA^{d} [Å^2]
Non-chlorinated^{d}	Control	*a-1*	−79	−102	4.30	665
	Modified dyes	*a-2*	−181	−161	−3.66	825
		a-3	−244	−211	−6.26	920
Chlorinated	Control^{d}	*b-1*	−82	−110	5.31	740
	Modified dyes	*b-2*	−92	−104	2.18	849
		b-3	−92	−104	2.18	849
		b-4	−205	−203	−0.38	999

^{a} ΔG_{w} in kJ mol^{-1}, is the solvation energy in water. ^{b} ΔG_{o} in kJ mol^{-1}, is the solvation energy in *n*-octanol. ^{c} Log $P_{\mathrm{o/w}}$ calculated without linker. The linker imparts similar effect to the studied dyes (variation of log $P_{\mathrm{o/w}}$ by including the linker: 1.96–2.59).[34] ^{d} The solvent (water) accessible surface area (SASA) of the entire dye is given in Angstroms square (Å^2). ^{a,b,c}Values of non-chlorinated and *b-1* were calculated in our previous study.[34]

hydrophilic dye among SQs in this study (log $P_{\mathrm{o/w}}$ = −6.26). *a-3* also had the largest SASA (920 Å^2) among the non-chlorinated SQs.

The chlorinated SQs *b-2* and *b-3* have *-buSl* at position 3′ and 3 in the indolenine rings, respectively, as compared with *b-1* (Fig. 2A). *b-2* and *b-3* have similar optical properties but their chemical structures are different because the position of the substituent change with respect to the position of the SQ-DNA linker. Specifically, the SQ-DNA linker and the *-buSl* substituent are located on the same indolenine ring in *b-2*, whereas the SQ-DNA linker and the *-buSl* substituent are located on different indolenine rings in *b-3* (Fig. 2A). The relative position of the *-buSl* substituent and SQ-DNA linker was purposely changed to investigate its influence on $J_{m,n}$. The *-buSl* substituent in *b-2* and *b-3* reduced the ΔG_{w} to −92 kJ mol^{-1} as compared with ΔG_{w} of *b-1* of −82 kJ mol^{-1}. The presence of *-buSl* in *b-2* and *b-3* also slightly increased ΔG_{o} to −104 kJ mol^{-1} as compared with ΔG_{o} of *b-1* of −110 kJ mol^{-1}. The slightly increased ΔG_{o} likely is due to the presence of the hydrophobic butyl chain in the *-buSl* substituent. Additionally, the log $P_{\mathrm{o/w}}$ was reduced from 5.31 in *b-1* to 2.18 in *b-2* and *b-3*, indicating an increased affinity to water of these two SQs. The larger SASA of *b-2* and *b-3* (849 Å^2) than *b-1* (740 Å^2) reflects the larger structural size of *-buSl* than *-Cl*. The symmetrically substituted *b-4* has *-buSl* in positions 3- and 3′ of the indolenine ring. *b-4* exhibited nearly two times the ΔG_{w} and ΔG_{o} of *b-1*, *b-2*, and *b-3*; the presence of a sulfonate group and a butyl chain in the *-buSl* substituent increased the ΔG_{w} and ΔG_{o}, respectively. The log $P_{\mathrm{o/w}}$ of *b-4* became slightly negative (−0.38) and SASA increased due to the presence of two *-buSl* substituents. Compared to the other chlorinated SQs, the close to zero value for the log $P_{\mathrm{o/w}}$ of *b-4* suggests its affinity to both polar and non-polar solvents due to presence of *-buSl* substituents. The presence of a *-buSl* substituent in *b-2* and *b-3* may also confer affinity to polar and non-polar solvents to these dyes, but with a smaller propensity as compared to *b-4*.

Finally, the presence of *-Sl* and *-buSl* substituents in the non-chlorinated dyes resulted in a larger reduction of log $P_{\mathrm{o/w}}$ as compared with the introduction of only *-buSl* substituents in the chlorinated SQs. These results indicate that *-Cl* enhanced the hydrophobic behavior of SQs and that the *-buSl* substituent imparted less hydrophilicity as compared with the *-Sl* group.

3.2. Characteristics squaraine dyes (SQs) substituents

The Hammett constant (σ) and *A*-value were used to compare the effect of substituent on electronic and steric effects, respectively. The electronic effect[61] described by σ relies on the inductive and resonance effects of the substituent in the benzene ring. The packing of SQs might rely on σ that represents the electronic effect of replacing *-H* with *-Cl* and *-Sl* on the aromatic rings. Substituents with a high electron-withdrawing capacity compared to *-H* (σ = 0) show positive σ values, while substituents having a high electron-donating capacity show negative values. For the present study, *para* position (σ_{p}) is pertinent because indolenine rings of SQs are substituted in position *para*, *e.g.*, from 4-chlorophenylhydrazine (SI 1†). According to σ_{p}, the substituents used in the present study are characterized by their moderate (*-Sl*) and weak (*-Cl*) electron-withdrawing capacity (Table 2).

The local bulkiness of the substituents is characterized by high *A*-value that quantifies the difference of conformational energy when the substituent is in the equatorial or axial position on cyclohexane. A previous study[43] found that the local bulkiness can be helpful in understanding trends in molecular packing. The DFT-calculated *A*-values of *-Cl* (0.47 kcal mol^{-1}), *-buSl* (1.83 kcal mol^{-1}), and *-Sl* (2.25 kcal mol^{-1}) showed that local bulkiness better reflects the spatial arrangement of the

Table 2 Characteristics of substituents of squaraine dyes (SQs)

Name	Chemical formula	Representation	*A*-value^{a} [kcal mol^{-1}]	$\sigma_{\mathrm{p}}{}^{b}$
Hydrogen	H	*-H*	0	0
Chlorine	Cl	*-Cl*	0.47	0.23
Butylsulfo	(CH$_2$)$_4$SO$_3$H	*-buSl*	1.83	n/a
Sulfo	SO$_3$H	*-Sl*	2.25	0.35

^{a} Calculated using DFT. ^{b} Hammett constant in position *para* (σ_{p}) was calculated by Hansch *et al.*[61] Hammett constant (σ) of SO$_3{}^{-}$ was used as a reference of SO$_3$H. n/a: σ for dyes *b-2* and *b-3* are not applicable because *-buSl* substituents are not conjugated with the indolenine rings of the SQs.

atoms on the substituents rather than the overall size of the substituent (Table 2). These results were compared with the control *-H* (*A*-value = 0). The *A*-value of *-Cl* calculated in the present study was close to a value previously reported in mono-substituted cyclohexane conformer, 0.51 kcal mol^{-1}.[62] Comparison of the *A*-value of *-buSl* in the present study was limited to the closest structure available in the literature of ethyl chain (*A*-value 1.79 kcal mol^{-1}).[63] The higher *A*-value of *-buSl* compared to the *A*-value of the ethyl chain in the literature[63] is ascribed to the presence of the additional ethylene and sulfo moieties.

Comparisons of the influences of substituent properties (σ and *A*-value) on the dye properties (log $P_{o/w}$ and SASA) were made using only symmetrically substituted *a-1*, *a-2*, and *b-1*, which have one substituent in each indolenine ring. Compared with *-Sl*, *-Cl* has a lower electron withdrawing capacity and it is less bulky. In regard to the properties of SQs, the hydrophilicity increased in the order *b-1* < *a-1* ≪ *a-2*, while SASA increases in the order *a-1* < *b-1* < *a-2*. Although the large molecular size of substituents increased SASA, it did not necessarily enhance the hydrophilicity of SQs because the latter depends on the presence of polar groups rather than molecular size. By coincidence, the *A*-value and SASA follow similar tendencies (Table 2); while *A*-value represents the energetic preference imparted by the substituents on cyclohexane for the equatorial position, SASA represents the physical size of a SQ.

3.3. Photophysical properties and exciton delocalization of SQ-DNA constructs

The optical characteristics of monomers and dimers of non-chlorinated and chlorinated SQs are briefly summarized to give a context to the KRM modeling results in section 3.4. Extended information regarding the steady-state optical characterization of monomers and aggregates of non-chlorinated SQs and *b-1* dye is reported in our previous study.[34] The propensity for aggregation of SQ dyes was confirmed by changes in their optical properties such as absorption and fluorescence spectra (Table 3 and Fig. 3, 4). The SQ monomers

attached to DNA-HJ showed absorption peaks between 638 and 649 nm, which are consistent with the main absorption peak of modified SQ dyes reported in previous studies[47,64] (Table 3 and section SI 3†). The *b-1* monomer exhibited a peak at 645 nm which is red-shifted relative to the peak at 638 nm in the unmodified *a-1* monomer. The presence of an electron-withdrawing *-Cl* substituent in *b-1* (Table 3) results in a red-shifted absorption spectrum.

Compared with the 638 nm absorption maximum of the *a-1* monomer control, non-chlorinated *a-2* exhibited a slightly red-shifted absorption peak at 640 nm and *a-3* showed a blue-shifted peak at 636 nm.[33] Compared with the 645 nm absorption maximum of the *b-1* monomer control, chlorinated SQs *b-2*, *b-3*, and *b-4* exhibited slightly red-shifted peaks at 647, 647, and 649 nm, respectively. The red-shifted effect upon the addition of *-buSl* substituents was also reported for free dyes;[47] that is, the dyes not tethered to DNA. Furthermore, it seems that the optical properties of chlorinated SQs are influenced by the electron-withdrawing ability of chlorine atoms, which may also potentially influence their aggregation propensity and $J_{m,n}$. This red-shift effect of *-Cl* substituent was also reported in previous studies of Cy5s[43] and SQs.[34]

All dimers exhibited a blue-shifted absorption peak relative to the lowest-energy monomer peak, which is a characteristic of H-aggregates.[1] The adjacent *b-4* dimer also exhibited a red-shifted absorption peak. Moreover, the amplitude of the absorption peak at high energy (noted as *A*2) was usually greater than the absorption peak at low energy (noted as *A*1), the latter of which aligns with the absorption maximum of the corresponding monomer (Fig. 3 and 4). The *A*2/*A*1 ratio determined from the absorption spectra, which can be used to gauge aggregation propensity or excitonic coupling assuming a single aggregation (H-aggregation), was higher in adjacent dimers (1.2–3.7) than in transverse dimers (0.6–2.0). These results indicate either stronger propensity for aggregation or stronger excitonic coupling in the adjacent dimers (Table 3). The generally lower *A*2/*A*1 ratio of the chlorinated dyes (0.6–0.9), of transverse dimers, is indicative of either a weaker propensity for aggregation or a weaker excitonic coupling.

Table 3 Optical properties of squaraine dyes (SQs) monomers and dimers

Dye group		SQ dye	Monomer Maximum peak (nm)	Adjacent dimer			Transverse dimer		
				Maximum peaks (nm)	*A*2/*A*1[a]	FS[b] [%]	Maximum peaks (nm)	*A*2/*A*1[a]	FS[b] [%]
Non-chlorinated	Control	*a-1*	638	592; 629	1.3	91	606; 632	0.8	87
	Modified dyes	*a-2*	640	598; 630	1.2	85	607; 630	1.2	90
		a-3	636	594; 631	1.3	69	596; 632	0.8	77
Chlorinated	Control	*b-1*	645	596; 633	3.7	93	600; 633	2.0	94
	Modified dyes	*b-2*	647	598; 632	3.3	72	601; 641	0.9	87
		b-3	647	599; 636	2.6	46	604; 641	0.6	73
		b-4	649	603; 638; 655	[c]	73	603; 643	0.6	76

Experiments were conducted at 1× TBE buffer, 15 mM MgCl$_2$ containing 1.5 µM DNA construct at room temperature (22 °C). Data of non-chlorinated and *b-1* dyes were calculated from absorption and fluorescence data presented in our previous study.[34] [a] *A*2/*A*1: is the ratio of absorbance peak at high energy (low wavelength)/absorbance peak at low energy (high wavelength) of experimental data (Fig. 3 and 4). [b] The fluorescence emission was scaled with absorptance to calculate the fluorescence suppression (FL) of dimer in reference to their monomers. [c] This structure showed three peaks (Fig. 3).

Fig. 3 Experimental and modeled absorption and circular dichroism (CD) spectra of non-chlorinated squaraine dyes (plot in first and third rows). 3D plots of transition dipole moments of dyes (blue and red arrows projected to *XY, YZ,* and *XZ* planes in black arrows) derived from the KRM modeling (plots in second and fourth rows). In heterogeneous aggregates, the distance between dimers is around 1 μm. Experimental data (absorption and CD) from our previous study[34] were used to refine the KRM modeling. "*A1*" indicates the low energy absorbance peak aligned with the monomer spectra, and "*A2*" represents the high energy absorbance peak that appears upon the formation of aggregates.

Fig. 4 Experimental and modeled absorption and circular dichroism (CD) spectra of the chlorinated squaraine dyes (plots in first and third rows). 3D plots of transition dipole moments of dyes (blue and red arrows projected to *XY*, *YZ*, and *XZ* planes in black arrows) derived from the KRM model-ing (plot in second and fourth rows). In heterogeneous aggregates, the distance between dimers is around 1 μm. Experimental data (absorption and CD) of *b-1* dimer was taken from our previous study.[34] "*A1*" indicates the low energy absorbance peak aligned with the monomer spectra, and "*A2*" represents the high energy absorbance peak that appears upon the formation of aggregates.

There is a noticeable effect on the absorption spectra of the adjacent dimers by changing the relative position of the *-buSl* substituent and SQ-DNA linker in the case of *b-2* and *b-3*. The *A2/A1* ratio is higher when the *-buSl* substituent and the SQ-DNA linker are attached to the same indolenine ring (*A2/A1* of *b-2* = 3.3) compared to when they are attached to rings on opposite sides (*A2/A1* of *b-3* = 2.6). *b-4* dimer showed three absorption peaks, which suggests a potential mixture of

Table 4 Geometric parameters of squaraine dye dimers calculated using the theoretical approach of the Kühn−Renger−May model (KRM model)

Attachment in DNA-HJ	Dye group		Dye label	$J_{m,n}$ [meV]	$R_{m,n}$ [nm]	$d_{m,n}$ [nm]	$\alpha_{m,n}$ [°]	θ_m [°]	θ_n [°]	θ_t [°]
Adjacent BC	Non-chlorinated	Control	a-1*	136	0.34	0.34	1	85	85	−1
				53	0.62	0.45	5	50	53	5
		Modified dyes	a-2*	47	0.70	0.65	4	78	76	3
				117	0.39	0.36	4	85	83	−3
			a-3*	48	0.87	0.37	41	43	85	−2
				109	0.44	0.42	2	88	86	−1
	Chlorinated	Control	b-1	132	0.34	0.34	1	89	89	−1
		Modified dyes	b-2	100	0.42	0.34	10	90	83	−7
			b-3	103	0.46	0.34	10	84	86	3
			b-4*	96	0.48	0.34	12	68	79	−6
				−41	1.46	0.35	84	43	41	0
Transverse AC	Non-chlorinated	Control	a-1	50	1.00	0.36	50	66	63	1
		Modified dyes	a-2	71	0.68	0.34	28	83	70	−5
			a-3	62	0.91	0.35	44	67	69	2
	Chlorinated	Control	b-1	79	0.56	0.34	17	75	88	3
		Modified dyes	b-2	62	0.73	0.34	34	66	82	9
			b-3	51	0.94	0.37	50	81	49	9
			b-4	51	0.96	0.37	52	80	48	9

$J_{m,n}$ is excitonic hopping parameter of dimers whose configuration is defined by the TDMs m and n. $R_{m,n}$ is the center-to-center dye distance. $d_{m,n}$ is the minimum distance between dyes; $\alpha_{m,n}$ is the angle between TDMs (supplementary if it is >90°); θ_m and θ_n are the slip angles of TDMs m and n. θ_t is the twist angle of the TDMs m and n. Fig. 2C depicts the geometrical relations for $R_{m,n}$, $d_{m,n}$, θ_m, θ_n, and θ_t. Star (*) indicates that these samples were modeled using the KRM model approach of two dimer subpopulations (multiple populations of dimers), which showed better fitting than the single dimer subpopulation approach. The sign of $J_{m,n}$ does not influence the result of processing the Hamiltonian equation because it is related to the orientation of the corresponding transition dipole moment (TDM) vector.

ensemble-level subpopulations with different dye packing arrangement (*e.g.*, H- and J-aggregates) that was further examined using the KRM modeling tool. We attribute the bands at 603 and 638 nm to H-aggregates and the band at 655 nm to J-aggregates (Fig. 4).

Adjacent dimers showed lower CD intensity compared to transverse dimers (Fig. 3 and 4). The difference of the SQ-DNA linker positions between *b-2* and *b-3* reduced the CD spectra intensity of these dimers and shifted the signature from negative to positive signal. The CD signal of aggregates relies on $J_{m,n}$, which is governed by the proximity and mutual orientation of TDMs.[33] A strong CD signal indicates excitonic interactions, whereas a weak signal does not necessarily preclude these interactions. A weak CD signal could also indicate that the ensemble-level sample consists of a heterogeneous mixture of dimer subpopulations with different packing configurations.[33] In fact, the formation of two aggregate subpopulations in the adjacent dimers of non-chlorinated SQs with different packing arrangements is supported by KRM modeling (section 3.4). The high intensity of the bisignate CD spectra of *b-2*, *b-3*, and *b-4* transverse dimers compared to the *b-1* transverse dimer indicates that the TDMs were twisted, which was confirmed by the KRM results (Table 4). The formation of J- and H-aggregates subpopulations in the case of *b-4* dimers is difficult to identify by analyzing only the CD spectra; as such, changes of the absorption spectra were also considered.

All dimer solutions exhibited fluorescence suppression relative to their monomer solutions. The fluorescence suppression was reduced as log$P_{\text{o/w}}$ decreased (increasing hydrophilicity) for non-chlorinated and chlorinated dyes, except for transverse

non-chlorinated dimers (Tables 3 and SI 4†). The emission detected in the dimer solutions is likely caused by a small subpopulation of highly emissive SQ monomers or "optical" monomers not forming an aggregate.[14] The different fluorescence suppression between *b-2* and *b-3* dimers reflects the effect of the SQ-DNA linker position in these SQs. The higher fluorescence suppression exhibited by *b-2* (72–87%) than *b-3* (46–73%) is consistent with the $A2/A1$ ratio derived from absorption spectra in these dimers. The effect on orientation and excitonic coupling strength by changing the attachment positions of the dyes was confirmed with the KRM modeling (section 3.4).

The aggregation tendencies of the SQs are consistent with the result of KRM modeling discussed in section 3.4. The photophysical changes of SQ dimers, such as blue-shifted absorption spectra relative to the corresponding monomer, were influenced by the geometrical arrangement of SQ dimers and are consistent with the characteristics of the type of aggregates described by Kasha based on the Frenkel exciton theory[1] (Fig. 1). The considerably quenched emission is consistent with enhanced nonradiative decay upon SQs aggregation, and the residual emission may arise from a small subpopulation of "optical" monomers.[14]

3.4. Geometry and excitonic delocalization of SQ dimers

The KRM modeling results showed that transverse *a-1*, *a-2*, *a-3*, and adjacent and transverse *b-1* dimers likely form a single population of aggregates; $J_{m,n}$ and dimer orientations agrees with our previous findings.[34] In contrast, adjacent dimers *a-1*, *a-2*, and *a-3* likely formed an ensemble-level mixture composed of different subpopulations of aggregates, where one subpopu-
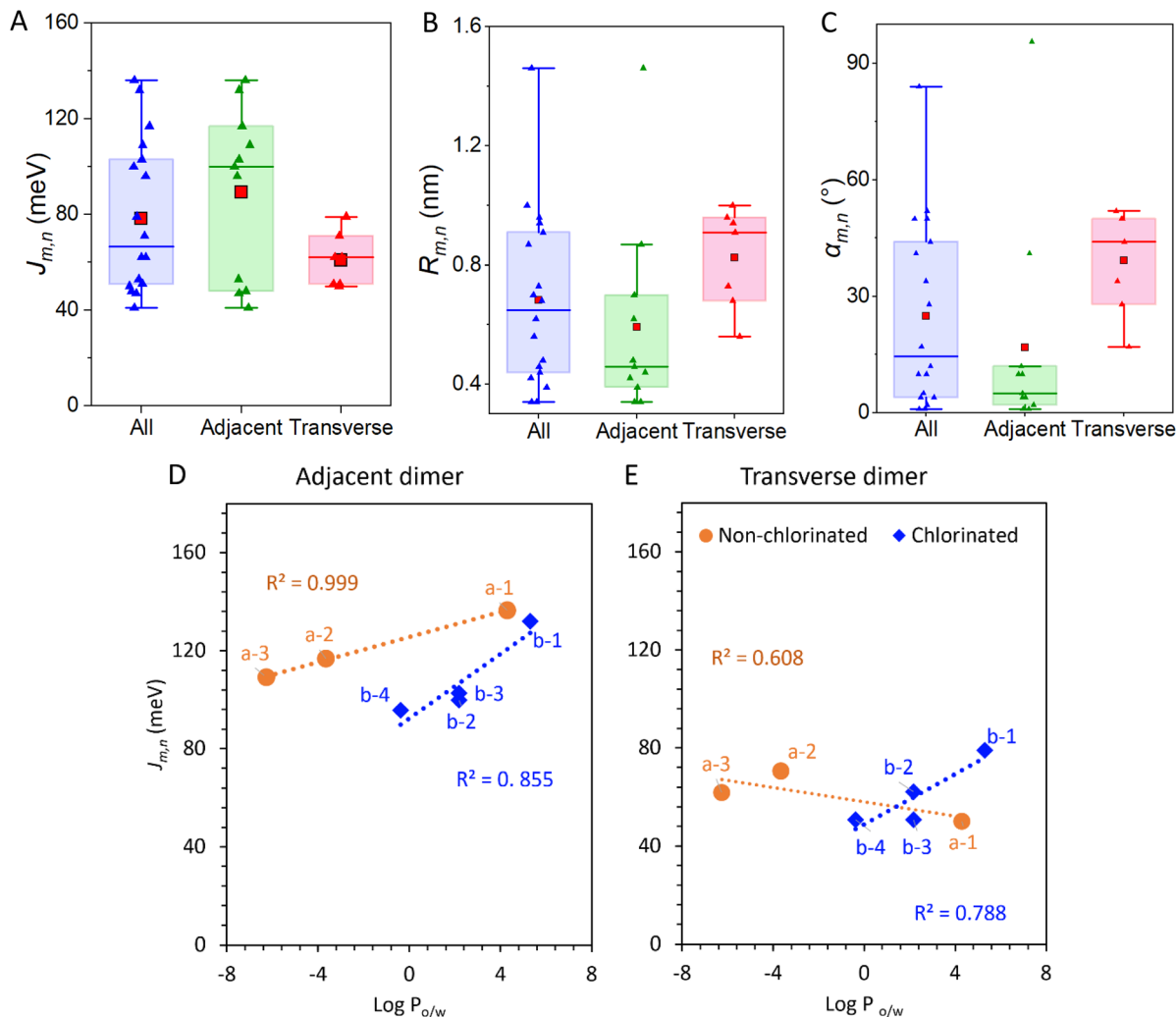
Fig. 5 (A) Excitonic hopping parameter ($J_{m,n}$), (B) center-to-center dye distance ($R_{m,n}$) and (C) angle between the transition dipole moments ($\alpha_{m,n}$) of squaraine dimers. In the boxplots, lower and upper values of the whiskers are the 5th and 75th percentiles; lower and upper extremes of the box are the 25th and 75th percentiles; line inside the box indicates the median value; and the red square (■) is the mean value of each data set. Relation between $J_{m,n}$ and hydrophobicity (log $P_{o/w}$) of adjacent (D) and transverse (E) squaraine dimers.

lation of aggregate exhibited two-fold higher $J_{m,n}$ with a shorter $R_{m,n}$ than the second subpopulation of aggregate (Table 4). Compared to the modeling approach for a single population of aggregates (approach of homogeneous population of aggregates[34]), the modeling approach requiring multiple subpopulations (heterogeneous type of aggregates approach) of a-1, a-2, and a-3 dimers improved the goodness of fit between the modeled and experimental absorption and CD spectra data (Fig. 3).

The orientation estimated using the KRM modeling showed that most dimers have non-parallel TDMs but still showed spectral features of H-aggregates (Fig. 2 and 3). Since the range of estimated $J_{m,n}$ values (41–136 meV) for SQ aggregates is broad, SQ dimers were differentiated in two groups using the median $J_{m,n}$ value of all SQ dimers investigated (66.5 meV). The group of dimers with $J_{m,n}$ smaller than the median (66.5 meV) were mainly represented by transverse dimers ($R_{m,n}$

= 0.73–1.00 nm and $\alpha_{m,n}$ = 34–52°) and dimers with a lower $J_{m,n}$ of heterogeneous aggregates ($R_{m,n}$ = 0.62–1.46 nm and $\alpha_{m,n}$ = 5–96°) (Fig. 5B and C). In contrast, the group of dimers with $J_{m,n}$ greater than the median value (66.5 meV) were mainly represented by adjacent dimers and transverse a-2 and b-1 dimers that exhibited $R_{m,n}$ between 0.34 and 0.68 nm and $\alpha_{m,n}$ between 1 and 28° (Fig. 5A).

The attachment position of the dyes in the DNA-HJ was one of the important factors influencing $J_{m,n}$ between and geometry of dyes in aggregates of all samples. In agreement with previous studies,[12,32–34,43] the present study demonstrated that the attachment position of SQs in the DNA-HJ impacts $J_{m,n}$ and geometry of dimers as follows. The adjacent dimers have $J_{m,n}$ greater than transverse dimers along with smaller $\alpha_{m,n}$ and $R_{m,n}$ (Table 4 and Fig. 5A–C), highlighting that the proximity of dyes plays an essential role in the strength of excitonic interaction. This dye proximity can be influenced by the attachment

Paper

point of the dye in the DNA. In the dye aggregates surveyed in the present study, large $R_{m,n}$ often results in large $\alpha_{m,n}$, with the latter dependent on the slip angles of each dye (θ_m and θ_n) and the twist angle (θ_t). The tendency for higher $J_{m,n}$ in adjacent dimers rather than transverse dimers may result from the physicochemical interaction of dyes with DNA templates as demonstrated at single molecule level.[31] Such interaction is driven by the unique physicochemical environment where the dyes reside.[65] The observed effect of the SQs position on the template is opposite to the one reported for substituted Cy5s,[43] in which transverse dimers exhibit a higher $J_{m,n}$ than adjacent dimers. The opposite $J_{m,n}$ results between SQs and Cy5s in adjacent and transverse positions in DNA-HJ may be due to the different linkers. While Cy5s in the cited study were attached to the DNA *via* two linkers that restrict the degrees of freedom, SQs in this study are attached to the DNA *via* single flexible linker covalently bound to a modified thymine base. Such attachment condition of SQs, in contrast to the Cy5s, may allow sufficient spatial freedom for the SQs to explore multiple dye packing configurations and potentially find the optimal configuration.

The control *a-1* and *b-1* dimers exhibited higher $J_{m,n}$ than dyes modified with sulfo substituents. Interestingly, the adjacent *b-1* dimers formed only one population of aggregates with $J_{m,n}$ = 132 meV. In contrast, the sample of adjacent *a-1* dimer formed a mixture of aggregates with $J_{m,n}$ = 136 and 53 meV. The KRM modeling approach of heterogeneous subpopulation of aggregates applied to *a-1* dimer showed an improved fit over that of the single dimer approach reported in our previous study[34] (Fig. 4, section SI 5.1 and SI 6†). Further studies are needed to elucidate the reasons leading to the formation of heterogenous subpopulations of the dimer. The electron-withdrawing ability of -*Cl* in *b-1* dimer may intensify the electrostatic attraction between indolenine rings of SQs and promote the formation of only one type of dimer population.[66,67]

The second important factor influencing $J_{m,n}$ between and geometry of dyes in aggregates of SQs is the hydrophilicity quantified by log $P_{o/w}$, which depends on the characteristics of substituents and their location on the dye. The substituents of SQs in this work are characterized by different amounts of local bulkiness and electron-withdrawing capabilities that have the potential to impact the molecular aggregation in solution (Table 2). The amphiphilic behavior of -*buSl* substituent on the dye core may impact the molecular packing. An asymmetric distribution of *buSl* substituents on the dye core may play an important role, especially when changing the dye-DNA linker. Below is described the effect of hydrophilic substituents of SQ dye for each non-chlorinated and chlorinated hydrophilic dyes.

The KRM modeling suggested that adjacent *a-2* and *a-3* dyes formed two dimer subpopulations, one exhibiting stronger coupling than the other (Table 4). Compared to the single dimer approach,[34] the heterogeneous subpopulation of aggregates approach improved the fitting between experimental and modeled data of *a-2* and *a-3* dimers (Fig. 4, section SI 5.1 and SI 6†). Solution of dimer *a-2* consisted of subpopulations of aggregates with $J_{m,n}$ = 117 and 47 meV. Solution of dimer *a-3*

consisted of subpopulations of aggregates with $J_{m,n}$ = 48 and 109 meV, which is similar to solutions of dimer *a-1*. The presence of two modeled subpopulations of aggregates in adjacent dimers but not in transverse dimers suggests that the position of the dyes in the DNA-HJ may play a role in the formation of heterogeneous type of aggregate. These results are consistent with observations of heterogeneity in aggregates of some adjacent dimers of Cy5 and limited heterogeneity in aggregates of transverse dimers of Cy5.[43,68] In most cases, heterogeneity of Cy5 adjacent dimers resulted in dimer pairs with opposite chirality though with similar packing.[43] Interestingly, chirality of single population of SQ dimers can be controlled by using different lengths of dye linkers.[69] The heterogeneity observed in adjacent dimers (*a-1*, *a-2*, *a-3*, and *b-4*) could result from two major conformations (Iso I and Iso II)[70] that DNA-HJs may still adopt when SQs are attached. In samples exhibiting heterogeneous aggregate populations, the dimer with high $J_{m,n}$ represents the maximum exciton interaction strength that can be achieved with a given dye properties. Therefore, the highest $J_{m,n}$ of each heterogeneous population was used to analyze the effect of dye hydrophilicity on exciton interaction strength.

As expected and in agreement with our hypothesis, a linear regression analysis showed that increased hydrophilicity reduces $J_{m,n}$ of adjacent dimers (R^2 = 0.999. Fig. 5D). Likewise, as hypothesized, larger $R_{m,n}$ was observed by increasing the SQs hydrophilicity. This result agrees with the finding in Stadler *et al.*[28] It also provides updated insight on our observation in aggregates of SQs featuring *Sl* and *buSl* substituents as reported in our previous study.[34] $J_{m,n}$ showed similar dependence on SASA (R^2 = 0.989) (section SI 7†) as hydrophilicity (R^2 = 0.999). However, for transverse dimers, there is no clear trend between hydrophilicity and $J_{m,n}$ (R^2 = 0.608. Fig. 5E). Many studies have demonstrated that hydrophobic interactions enhance dye aggregation[28,71] because it promotes π–π stacking.[72,73] Therefore, the modest reduction of $J_{m,n}$ upon adding *buSl* substituents may be related to increased electrostatic and/or steric repulsion of SQs. For example, electrostatic repulsion between sulfo substituents and/or steric repulsion of sulfo butyl substituents may increase the intermolecular distance, reducing intermolecular interactions, which decreases excitonic coupling as supported by the KRM modeling results for adjacent dimers. Hence, the findings from the adjacent dimers of SQ dyes in this study support a general trend that increasing hydrophilicity decreases $J_{m,n}$. Moreover, these results build upon and update the KRM modeling of SQ dyes reported in our previous study.[34] The present study provides a mean of analysis of the structural heterogeneity at the ensemble-level of these SQs. Further investigations are needed to elucidate the factors influencing $J_{m,n}$ of non-chlorinated transverse dimers. It appears that hydrophilicity is not the main factor governing dye aggregation.

According to the KRM modeling results, solutions of chlorinated SQ dimers consisted of a single population of aggregate type, except for adjacent dimer *b-4*. Compared to the -*H* substituent of non-chlorinated dyes, -*Cl* is a bulkier substituent (A-value = 0.47 kcal mol^{-1}) and has a weak electron-withdraw-

ing capacity (σ_p = 0.23). These two characteristics of -*Cl*, combined with neutral charge impart hydrophobic properties to the dye, which might promote the formation of a single population of aggregate type. Hydrophobic interactions enhance the π–π stacking as discussed above. Compared to adjacent chlorinated dimers, transverse chlorinated dimers showed a lower $J_{m,n}$ with a higher θ_t (Table 4) that derives from the high intensity of CD spectra depicted in Fig. 4, indicating that the TDMs are not perfectly parallel. Unlike transverse dimers, adjacent dimers *b-2* ($J_{m,n}$ = 100 meV) and *b-3* ($J_{m,n}$ = 103 meV) showed similar excitonic interaction strengths. This result was expected because dyes *b-2* and *b-3* have the same hydrophilic properties but different positions of the SQ-DNA linker. Surprisingly, transverse *b-2* ($J_{m,n}$ = 71 meV) and *b-3* ($J_{m,n}$ = 62 meV) dimers showed slightly different $J_{m,n}$; that may result from the combined effect of the position of the SQ-DNA linker and SQs in the DNA-HJ. This result suggests that the attachment positions of dyes in the DNA-HJ and in the SQ-DNA linker in the SQ could contribute to changes in the molecular packing.

Interestingly, our modeling indicated that solutions of the adjacent dimer *b-4* consisted of a mixture of two subpopulations of aggregates. The red-shifted and blue-shifted absorption spectra depicted by dimer *b-4* relative to its monomer (Fig. 4) prompted an intensive KRM modeling work using multiple subpopulations to model the heterogeneous population at the ensemble-level. The results suggested that dimer *b-4* forms population of aggregates with $J_{m,n}$ = 96 meV that has a minimum intermolecular distance ($d_{m,n}$) 0.34 nm, and another with $J_{m,n}$ = −41 meV that has $d_{m,n}$ = 0.35 nm. The mixture of aggregates subpopulations might result from more hydrophilic behavior *b-4* due to the two hydrophilicity imparting substituents -*buSl* as compared with *b-2* and *b-3* with a single -*buSl* (Table 2). Given the current limitation of our KRM tool to tune the ratio of subpopulations of aggregates, the accurate estimation of the ratio of aggregate types remains challenging. The estimation of dye orientations and aggregate types ratios within a population would be possible in future studies using new approaches and methods of KRM modeling tool that involves the combination of experiments and theory.

Increasing the dye hydrophilicity of chlorinated dyes *via* the presence of sulfo substituents led to a larger $R_{m,n}$ and resulted in a smaller $J_{m,n}$. Using the maximum $J_{m,n}$ that was observed in *b-4*, the linear regression analysis confirmed that hydrophilicity reduces excitonic interaction strength of adjacent (R^2 = 0.855) and transverse (R^2 = 0.788) dimers of chlorinated SQs (Fig. 5D and E). $J_{m,n}$ of adjacent (R^2 = 0.711) and transverse (R^2 = 0.672) dimers showed a lower dependency on SASA (section SI 7†). The latter result agrees with the finding for non-chlorinated dyes that $\log P_{o/w}$ is a better predictor of $J_{m,n}$, as compared with SASA. Results of chlorinated dimers reconfirm the hypothesis that hydrophilicity reduces $J_{m,n}$ because sulfo substituents enhance the dye solubility and enlarge the intermolecular distance as discussed above. Findings of Guckian *et al.*[72] on aggregation of dyes non-covalently bound to DNA support that other factors such as dipole moment, polarizabil-

ity, and surface area are less important factors than hydrophobicity in stabilizing molecular packing.

Dimers with the symmetric distribution of substituents -*H* (*a-1*; control), -*Sl* (*a-2*), and -*Cl* (*b-1*) were further analyzed to gain better insight into the effect of substituents on $J_{m,n}$. The *b-4* dimer was not included in this analysis to avoid bias due to the -*Cl* and -*buSl* substituents in each indolenine ring. The substituents of SQs, with different local bulkiness (*A*-value) and electron-withdrawing capacity (Hammett constant, σ), conferred a unique water affinity and SASA to SQs. The *A*-value of substituents increased as SASA increased, though this relation does not indicate causation. That is because *A*-value indicates the difference between the energies of equatorial and axial cyclohexane conformation resulting from the presence of a substituents while SASA is the solvent accessible area of SQ. σ did not show a trend with SASA or hydrophilicity. There was no clear trend of $J_{m,n}$ by increasing the hydrophilicity of the three symmetrically substituted dyes. Interestingly, a negative relationship was observed between the *A*-value and $J_{m,n}$ of adjacent dimers (R^2 = 0.9998); in other words, $J_{m,n}$ decreased as the local bulkiness of the substituents increased (section SI 8†). The unclear trend observed in transverse dimers (R^2 = 0.191) requires further investigation to elucidate the factors affecting $J_{m,n}$. One possible explanation is the interaction of dyes with neighboring bases. The result of adjacent dimers indicates that after the hydrophilicity of SQs, *A*-value is a third factor potentially influencing $J_{m,n}$.

While results in the present study showed that the local bulkiness of substituents reduces $J_{m,n}$ between SQs in SQ dimers, a previous study found that bulkiness enhances $J_{m,n}$ between Cy5-R dyes in Cy5-R dimers (R: substituents).[43] One possible reason for the opposite trend between SQs and Cy5-R dimers when comparing $J_{m,n}$ and *A*-value could be due to the different water affinity of dye substituents. The bulky *tert*-butyl substituent of Cy5-R[43] has hydrophobic properties that enhance π–π interactions while the bulky -*Sl* substituent of SQs is hydrophilic which enhances the affinity of dyes to water and inhibits molecular aggregation. This opposite physical property of substituents influences the behaviors of SQs in solution and impacts their aggregation. Therefore, the influence of local bulkiness on the excitonic interaction strength of Cy5-R and SQ dimers follow different trends. Overall, the dyes featuring hydrophilic and amphiphilic substituents used in the present study exhibit high $J_{m,n}$ that can potentially be exploited for developing molecular quantum materials given their solution processability.

4.   Conclusions

This study demonstrated that non-chlorinated and chlorinated SQs with hydrophilic-imparting -*Sl* and -*buSl* substituents readily form dimer aggregates when templated using DNA. These SQ dimer aggregates showed different degrees of excitonic interaction strengths. One of the most important factors determining the geometry and excitonic hopping parameter

$(J_{m,n})$ is the attachment position of dyes in the DNA-HJ. For example, all adjacent dimers showed higher $J_{m,n}$ than the transverse dimers. The second important factor is the hydrophilicity of SQs ($\log P_{\mathrm{o/w}}$), which increases by adding -*Sl* and -*buSl* substituents, but also influenced by the presence of -*Cl* substituents. Therefore, the SQs were divided into non-chlorinated and chlorinated groups and analyzed separately. Increased hydrophilicity of non-chlorinated and chlorinated groups reduced $J_{m,n}$ because the -*Sl* and *buSl* substituents promoted the dye solubility in water that enlarges the intermolecular distance hindering aggregation. The third important factor could be the local bulkiness of the substituents. Additional factors such as SASA and electron-withdrawing capacity appear to play less important roles in the packing of the molecular aggregates. However, further investigation is needed to elucidate the factors influencing the $J_{m,n}$ of non-chlorinated transverse dimers. Hence, the finding of the present study bridges to new exciting leading-edge technologies using dye with hydrophilic-imparting substituents for developing molecular quantum materials.

The KRM tool was used to model heterogeneous populations formed by adjacent *a-1*, *a-2*, *a-3*, and *b-4* dimers. The presence of multiple subpopulations formed by SQs suggested by the KRM modeling opens research directions to further interrogate heterogeneous subpopulations using excitation-wavelength dependent steady-state and time-resolved spectroscopies. Likewise, single molecule investigations could allow the quantification of populations and their evolution over time. Reducing the heterogeneity of dye aggregates while maintaining their strong excitonic interactions are challenges that need to be addressed to improve control of exciton delocalization and application in quantum information systems.

Author contributions

Investigation: GP and JL. Dye design: OAM, RDP, and JL. Dye synthesis: EAT, AT, OMO, and AIK. Modeling of dye properties: GB and LL. Sample preparation and experiments: CKW and OAM. KRM code developing and modeling: BY, SR, and GP. Data curation and formal analysis: GP, SR, and KC-S. Original draft: GP and JL. Funding: JL, RDP, LL, OAM, and WBK. All authors: writing – review and editing.

Conflicts of interest

E.A.T. is the managing director of SETA BioMedicals, which has an interest in this project. Other authors have no conflicts to declare.

Acknowledgements

References

1 M. Kasha, *Radiation Research*, 1963, **20**, 55–70.

2 T. Mirkovic, E. E. Ostroumov, J. M. Anna, R. Van Grondelle, Govindjee and G. D. Scholes, *Chem. Rev.*, 2017, **117**, 249–293.

3 F. Fassioli, R. Dinshaw, P. C. Arpin and G. D. Scholes, *J. R. Soc., Interface*, 2014, **11**, 20130901.

4 B. Yurke, R. Elliott and A. Sup, *Phys. Rev. A*, 2023, **107**, 12603.

5 A. Huijser, P. L. Marek, T. J. Savenije, L. D. A. Siebbeles, T. Scherer, R. Hauschild, J. Szmytkowski, H. Kalt, H. Hahn and T. S. Balaban, *J. Phys. Chem. C*, 2007, **111**, 11726–11733.

6 B. Yurke and W. Kuang, *Phys. Rev. A*, 2010, **81**, 033814.

7 C. Laboda, H. Duschl and C. L. Dwyer, *Acc. Chem. Res.*, 2014, **47**, 1816–1824.

8 B. Yurke, in *Natural Computing Series*, eds. Janoska and N. and Winfree E., Springer Science and Business Media Deutschland GmbH, Singapore, 2023, vol. Part F821, pp. 125–169.

9 A. S. Klymchenko, *Acc. Chem. Res.*, 2017, **50**, 366–375.

10 P. Zhang, M. S. Zhu, H. Luo, Q. Zhang, L. E. Guo, Z. Li and Y. B. Jiang, *Anal. Chem.*, 2017, **89**, 6210–6215.

11 D. Mathur, S. A. Díaz, N. Hildebrandt, R. D. Pensack, B. Yurke, A. Biaggne, L. Li, J. S. Melinger, M. G. Ancona, W. B. Knowlton and I. L. Medintz, *Chem. Soc. Rev.*, 2023, **52**, 7848–7948.

12 O. A. Mass, C. K. Wilson, S. K. Roy, M. S. Barclay, L. K. Patten, E. A. Terpetschnig, J. Lee, R. D. Pensack, B. Yurke and W. B. Knowlton, *J. Phys. Chem. B*, 2020, **124**, 9636–9647.

13 N. J. Hestand and F. C. Spano, *Chem. Rev.*, 2018, **118**, 7069–7163.

14 J. S. Huff, P. H. Davis, A. Christy, D. L. Kellis, N. Kandadai, Z. S. D. Toa, G. D. Scholes, B. Yurke, W. B. Knowlton and R. D. Pensack, *J. Phys. Chem. Lett.*, 2019, **10**, 2386–2392.

15 B. L. Cannon, D. L. Kellis, L. K. Patten, P. H. Davis, J. Lee, E. Graugnard, B. Yurke and W. B. Knowlton, *J. Phys. Chem. A*, 2017, **17**, 6905–6916.

16 U. Rösch, S. Yao, R. Wortmann and F. Würthner, *Angew. Chem., Int. Ed.*, 2006, **45**, 7026–7030.

17 C. Zheng, C. Zhong, C. J. Collison and F. C. Spano, *J. Phys. Chem. C*, 2019, **123**, 3203–3215.

18 A. K. Singh, M. Fairoos, M. Kavungathodi, A. J. Mozer, K. Krishnamoorthy and J. Nithyanandhan, *Langmuir*, 2022, **38**, 14808–14818.

19 W. J. Harrison, D. L. Mateer and G. J. T. Tiddy, *J. Phys. Chem.*, 1996, **100**, 2310–2321.

20 I. G. Scheblykin, M. M. Bataiev, M. Van Der Auweraer and A. G. Vitukhnovsky, *Chem. Phys. Lett.*, 2000, **316**, 37–44.

21 R. F. Khairutdinov and N. Serpone, *J. Phys. Chem.*, 1995, **99**, 11952–11958.

22 Y.-C. Cheng and G. R. Fleming, *Annu. Rev. Phys. Chem.*, 2009, **60**, 241–262.

23 N. C. Seeman, *Nature*, 2003, **421**, 427–431.

24 B. Yurke, A. J. Turberfield, A. P. Mills Jr, F. C. Simmel and J. L. Neumann, *Nature*, 2000, **406**, 605–608.

25 N. C. Seeman, *Annu. Rev. Biochem.*, 2010, **79**, 65–87.

26 V. L. Malinovskii, D. Wenger and R. Haner, *Chem. Soc. Rev.*, 2010, **39**, 410–422.

27 A. L. Benvin, Y. Creeger, G. W. Fisher, B. Ballou, A. S. Waggoner and B. A. Armitage, *J. Am. Chem. Soc.*, 2007, **129**, 2025–2034.

28 A. L. Stadler, B. R. Renikuntla, D. Yaron, A. S. Fang and B. A. Armitage, *Langmuir*, 2011, **27**, 1472–1479.

29 R. A. Garoff, E. A. Litzinger, R. E. Connor, I. Fishman and B. A. Armitage, *Langmuir*, 2002, **18**, 6330–6337.

30 H. Asanuma, K. Shirasuka, T. Takarada, H. Kashida and M. Komiyama, *J. Am. Chem. Soc.*, 2003, **125**, 2217–2223.

31 K. Cervantes-Salguero, A. Biaggne, J. M. Youngsman, B. M. Ward, Y. C. Kim, L. Li, J. A. Hall, W. B. Knowlton, E. Graugnard and W. Kuang, *Int. J. Mol. Sci.*, 2022, **23**, 7690.

32 B. L. Cannon, L. K. Patten, D. L. Kellis, P. H. Davis, J. Lee, E. Graugnard, B. Yurke and W. B. Knowlton, *J. Phys. Chem. A*, 2018, **122**, 2086–2095.

33 S. K. Roy, O. A. Mass, D. L. Kellis, C. K. Wilson, J. A. Hall, B. Yurke and W. B. Knowlton, *J. Phys. Chem. B*, 2021, **125**, 13670–13684.

34 O. A. Mass, C. K. Wilson, G. Barcenas, E. A. Terpetschnig, O. M. Obukhova, O. S. Kolosova, A. L. Tatarets, L. Li, B. Yurke, W. B. Knowlton, R. D. Pensack and J. Lee, *J. Phys. Chem. C*, 2022, **126**, 3475–3488.

35 J. S. Huff, S. A. Díaz, M. S. Barclay, A. U. Chowdhury, M. Chiriboga, G. A. Ellis, D. Mathur, L. K. Patten, S. K. Roy, A. Sup, A. Biaggne, B. S. Rolczynski, P. D. Cunningham, L. Li, J. Lee, P. H. Davis, B. Yurke, W. B. Knowlton, I. L. Medintz, D. B. Turner, J. S. Melinger and R. D. Pensack, *J. Phys. Chem. C*, 2022, **126**, 17164–17175.

36 B. S. Rolczynski, S. A. Díaz, Y. C. Kim, I. L. Medintz, P. D. Cunningham and J. S. Melinger, *J. Phys. Chem. A*, 2021, **125**, 9632–9644.

37 M. Chiriboga, S. A. Diaz, D. Mathur, D. A. Hastman, J. S. Melinger, R. Veneziano and I. L. Medintz, *J. Phys. Chem. B*, 2022, **126**, 110–122.

38 M. I. Sorour, K. A. Kistler, A. H. Marcus and S. Matsika, *J. Phys. Chem. A*, 2021, **125**, 7852–7866.

39 S. M. Hart, J. L. Banal, M. A. Castellanos, L. Markova, Y. Vyborna, J. Gorman, A. P. Willard, M. Bathe and G. S. Schlau-Cohen, *Chem. Sci.*, 2022, **13**, 13020–13031.

40 S. M. Hart, W. J. Chen, J. L. Banal, R. Hä, M. Bathe, G. S. Schlau-Cohen, W. P. Bricker, A. Dodin, L. Markova, Y. Vyborna and A. P. Willard, *Chem*, 2020, **7**, 752–773.

41 L. I. Markova, V. L. Malinovskii, L. D. Patsenker and R. Häner, *Org. Biomol. Chem.*, 2012, **10**, 8944–8947.

42 F. Nicoli, M. K. Roos, E. A. Hemmig, M. Di Antonio, R. De Vivie-Riedle and T. Liedl, *J. Phys. Chem. A*, 2016, **120**, 9941–9947.

43 S. A. Díaz, G. Pascual, L. K. Patten, S. K. Roy, A. Meares, M. Chiriboga, K. Susumu, W. B. Knowlton, P. D. Cunningham, D. Mathur, B. Yurke, I. L. Medintz, J. Lee and J. S. Melinger, *Nanoscale*, 2023, **15**, 3284–3299.

44 L. I. Markova, V. L. Malinovskii, L. D. Patsenker and R. Häner, *Chem. Commun.*, 2013, **49**, 5298–5300.

45 B. Ananda Rao, H. Kim and Y. A. Son, *Sens. Actuators, B*, 2013, **188**, 847–856.

46 S. Sreejith, P. Carol, P. Chithra and A. Ajayaghosh, *J. Mater. Chem.*, 2008, **18**, 264–274.

47 L. I. Markova, E. A. Terpetschnig and L. D. Patsenker, *Dyes Pigm.*, 2013, **99**, 561–570.

48 K. Ilina, W. M. Maccuaig, M. Laramie, J. N. Jeouty, L. R. Mcnally and M. Henary, *Bioconjugate Chem.*, 2020, **31**, 194–213.

49 L. Kringle, N. P. D. Sawaya, J. Widom, C. Adams, M. G. Raymer, A. Aspuru-Guzik and A. H. Marcus, *J. Chem. Phys.*, 2018, **148**, 85101.

50 O. Kühn, T. Renger and V. May, *Chem. Phys.*, 1996, **204**, 99–114.

51 N. M. Garrido, I. G. Economou, A. J. Queimada, M. Jorge and E. A. Macedo, *AIChE J.*, 2012, **58**, 1929–1938.

52 M. J. Frisch, H. B. Schlegel, G. E. Scuseria, M. A. Robb, J. R. Cheeseman, G. Scalmani, V. Barone, F. G. A. Petersson, H. Nakatsuji, X. Li, M. Caricato, A. V. Marenich, J. Bloino, B. G. Janesko, R. Gomperts, B. Mennucci, H. P. Hratchian, J. V. Ortiz, A. F. Izmaylov, J. L. Sonnenberg, D. Williams-Young, F. Ding, F. Lipparini, F. Egidi, J. Goings, B. Peng, A. Petrone, T. Henderson, D. Ranasinghe, V. G. Zakrzewski, J. Gao, N. Rega, G. Zheng, W. Liang, M. Hada, M. Ehara, K. Toyota, R. Fukuda, J. Hasegawa, M. Ishida, T. Nakajima, Y. Honda, O. Kitao, H. Nakai, T. Vreven, K. Throssell, J. A. Montgomery, J. E. Peralta, F. Ogliaro, M. J. Bearpark, J. J. Heyd, E. N. Brothers, K. N. Kudin, V. N. Staroverov, T. A. Keith, R. Kobayashi, J. Normand, K. Raghavachari, A. P. Rendell, J. C. Burant, S. S. Iyengar, J. Tomasi, M. Cossi, J. M. Millam, M. Klene, C. Adamo, R. Cammi, J. W. Ochterski, R. L. Martin, K. Morokuma, O. Farkas, J. B. Foresman, D. J. Fox, G. W. Trucks, V. Barone and G. A. Petersson, Gaussian16 Revision A.03, 2016.

53 G. Barcenas, A. Biaggne, O. A. Mass, C. K. Wilson, O. M. Obukhova, O. S. Kolosova, A. L. Tatarets, E. Terpetschnig, R. D. Pensack, J. Lee, W. B. Knowlton, B. Yurke and L. Li, *RSC Adv.*, 2021, **11**, 19029–19040.

54 A. K. Rappe, C. J. Casewit, K. S. Colwell, W. A. Goddard and W. M. Skiff, *J. Am. Chem. Soc.*, 1992, **114**, 10024–10035.

55 M. D. Hanwell, D. E. Curtis, D. C. Lonie, T. Vandermeerschd, E. Zurek and G. R. Hutchison, *J. Cheminform.*, 2012, **4**, 17.

56 Y. Zhao and D. G. Truhlar, *Theor. Chem. Acc.*, 2008, **120**, 215–241.

57 T. D. Goddard, C. C. Huang, E. C. Meng, E. F. Pettersen, G. S. Couch, J. H. Morris and T. E. Ferrin, *Protein Sci.*, 2018, **27**, 14–25.

58 N. M. O'Boyle, A. L. Tenderholt and K. M. Langner, *J. Comput. Chem.*, 2008, **29**, 839–845.

59 E. Freytag, L. Kreimendahl, M. Holzapfel, J. Petersen, H. Lackinger, M. Stolte, F. Würthner, R. Mitric and C. Lambert, *J. Org. Chem.*, 2023, **88**, 10777–10788.

60 P. F. Santos, L. V. Reis, P. Almeida and D. E. Lynch, *CrystEngComm*, 2011, **13**, 1333–1338.

61 C. Hansch, A. Leo and R. W. Taft, *Chem. Rev.*, 1991, **91**, 165–195.

62 H.-J. Schneider and V. Hoppen, *J. Org. Chem.*, 1978, **43**, 3866–3873.

63 S. E. Boiadjiev and D. A. Lightner, *J. Am. Chem. Soc.*, 2000, **122**, 11328–11339.

64 U. Mayerhöffer, M. Gsänger, M. Stolte, B. Fimmel and F. Würthner, *Chem. – Eur. J.*, 2013, **19**, 218–232.

65 J. N. Wilson, J. Wigenius, D. R. G. Pitter, Y. Qiu, M. Abrahamsson and F. Westerlund, *J. Phys. Chem. B*, 2013, **117**, 12000–12006.

66 M. Watt, L. K. E. Hardebeck, C. C. Kirkpatrick and M. Lewis, *J. Am. Chem. Soc.*, 2011, **133**, 3854–3862.

67 E. G. Hohenstein, J. Duan and D. Sherrill, *J. Am. Chem. Soc.*, 2011, **133**, 13244–13247.

68 J. S. Huff, D. B. Turner, O. A. Mass, L. K. Patten, C. K. Wilson, S. K. Roy, M. S. Barclay, B. Yurke, W. B. Knowlton, P. H. Davis and R. D. Pensack, *J. Phys. Chem. B*, 2021, **125**, 10240–10259.

69 O. A. Mass, S. Basu, L. K. Patten, E. A. Terpetschnig, A. I. Krivoshey, A. L. Tatarets, R. D. Pensack, B. Yurke, W. B. Knowlton and J. Lee, *J. Phys. Chem. Lett.*, 2022, **2022**, 10688–10696.

70 C. Hyeon, J. Lee, J. Yoon, S. Hohng and D. Thirumalai, *Nat. Chem.*, 2012, **4**, 907–914.

71 K. Umezawa, D. Citterio and K. Suzuki, *Anal. Sci.*, 2008, **24**, 213–217.

72 K. M. Guckian, B. A. Schweitzer, R. X.-F. Ren, C. J. Sheils, D. C. Tahmassebi and E. T. Kool, *J. Am. Chem. Soc.*, 2000, **122**, 2213–2222.

73 K. M. Guckian, B. A. Schweitzer, R. X.-F. Ren, C. J. Sheils, P. L. Paris, D. C. Tahmassebi and E. T. Kool, *J. Am. Chem. Soc.*, 1996, **118**, 8182–8183.